Parallel and Multivalued Logic by the Two-Dimensional Photon-Echo Response of a Rhodamine−DNA Complex

Barbara Fresch,[†] Marco Cipolloni,[‡] Tian-Min Yan,[†] Elisabetta Collini,[‡] R. D. Levine,[§] and F. Remacle*,[†]

[†]Department of Chemistry, University of Liege, B4000 Liege, Belgium
[‡]Department of Chemical Sciences, University of Padova, 35131 Padova, Italy
[§]The Fritz Haber Research Center, The Hebrew University of Jerusalem, Jerusalem 91904, Israel

S *Supporting Information*

ABSTRACT: Implementing parallel and multivalued logic operations at the molecular scale has the potential to improve the miniaturization and efficiency of a new generation of nanoscale computing devices. Two-dimensional photon-echo spectroscopy is capable of resolving dynamical pathways on electronic and vibrational molecular states. We experimentally demonstrate the implementation of molecular decision trees, logic operations where all possible values of inputs are processed in parallel and the outputs are read simultaneously, by probing the laser-induced dynamics of populations and coherences in a rhodamine dye mounted on a short DNA duplex. The inputs are provided by the bilinear interactions between the molecule and the laser pulses, and the output values are read from the two-dimensional molecular response at specific frequencies. Our results highlights how ultrafast dynamics between multiple molecular states induced by light−matter interactions can be used as an advantage for performing complex logic operations in parallel, operations that are faster than electrical switching.
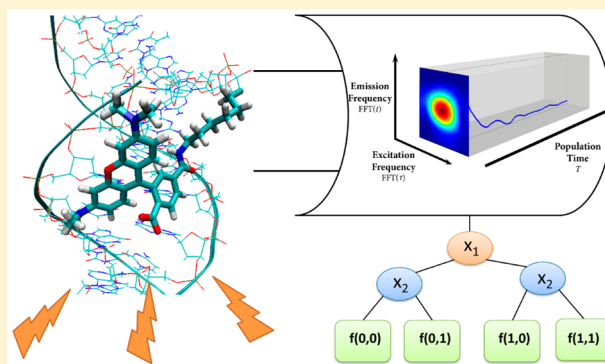
The interaction between molecules and optical signals allows the implementation of logic gates[1−4] and even more elaborate circuits as half[5] and full adder,[6,7] keypad lock,[8] and molecular sensors[9] at the molecular scale. Here, we demonstrate a two-dimension photon-echo (2D-PE) setup that allows evaluation of a multivariable logic function in parallel for all inputs and that delivers a macroscopic readout. This experimental realization is grounded in the scheme for parallel molecular processing by coherent 2D spectroscopy proposed in refs 10 and 11. The proposed optically addressed molecular device computes in parallel both binary and multivalued logic functions, taking advantage of the complex dynamics induced by the interaction of the molecular states with three successive optical pulses. Parallel processing is based on the capability of the 2D-PE to excite multiple transitions and to provide information on the coherent electronic and vibrational dynamics of the chromophoric system. The technique provides access to a significantly greater number of probes than conventional steady-state linear optical measurements, thereby enabling the implementation of parallel computing by observables.[12] The logic function that is computed can be designed by choosing a system with the required level structure and transition dipole patterns and/or by optimizing the parameters of the pulse sequence.[10] We report implementing logic on a 5′-carboxy-tetramethylrhodamine mounted on a short DNA duplex of 28 base pairs (TAMRA_DNA). We show below that being able to characterize and model the vibronic

response of this single chromophore allows computation of the molecular trees of three variable Boolean functions, as well as four valued functions. This unit is also a potential building block because the DNA duplex can be used as a scaffold to assemble multichromophoric systems with finely tunable properties.[13] Experimentally characterizing a vibronic structure for each chromophore exponentially increases the amount of information that can be processed in parallel. Details about sample preparation and 2D-PE optical measurements are reported in section 1 of the Supporting Information (SI).

2D-PE spectroscopy uses three ultrashort laser pulses to induce multiple transitions between excited molecular energy levels. The time evolution of the system is described by the density matrix, $\rho(t)$, whose diagonal and off-diagonal elements represent the populations and the coherences of the energy levels. In the experimental scheme shown in Figure 1a, the three wave vectors of the laser pulses exciting the sample at times τ_1, τ_2, and τ_3 are denoted as $\mathbf{k}_1$, $\mathbf{k}_2$, and $\mathbf{k}_3$, respectively. The PE signal is observed after the third laser−matter interaction in the phase-matching direction, $\mathbf{k}_{PE} = -\mathbf{k}_1 + \mathbf{k}_2 + \mathbf{k}_3$, and depends on the three positive delay times between successive laser pulses: the coherence time, $\tau = \tau_2 - \tau_1$, the population time, $T = \tau_3 - \tau_2$, and the detection time, t. The 2D-
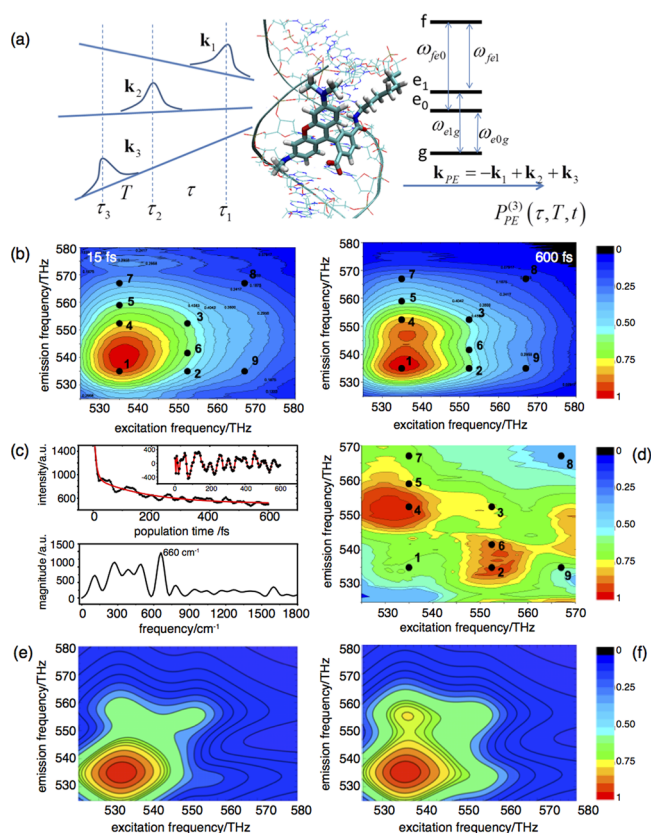
Figure 1. (a) Schematic representation of the 2D-PE pulse sequence exciting the TAMRA_DNA sample. (Right) Energy levels involved in the dynamics. (b) Experimental normalized rephasing 2D-PE spectra (absolute value) at a short ($T = 15$ fs) and longer ($T = 600$ fs) population time. The spectral positions corresponding to different transitions are numbered. (c) The upper-left panel shows the raw time trace taken from the lower cross-peak (552.4 THz, 535 THz, peak 2); in the inset, the residuals of the biexponential fit performed on the raw kinetic are reported. The lower panel shows the FT trace of the residuals. (d) The FT map shows the amplitude distribution of the beating component with frequency 660 cm^{-1} as a function of emission and excitation frequency. (e,f) Spectra (absolute value) simulated by propagating the density matrix for $T = 15$ and 600 fs; see section 5 of the SI for details.

PE spectrum is obtained as the double Fourier transform (FT) of the PE signal with respect to the coherence time ($\tau \rightarrow \omega_1$) and the detection time ($t \rightarrow \omega_2$). The 2D spectrum resolves the dynamics of the system along the excitation (ω_1) and the emission (ω_2) frequencies for each population evolution time T. Figure 1b reports two experimental 2D maps at short (15 fs) and longer (600 fs) population times. Qualitatively, the maps are characterized by a feature centered at 535 THz (position 1), in good agreement with the energy of the main S0−S1 electronic transition, giving rise to the maximum in the absorption spectrum (see section 2 of the SI). At early times T, this diagonal peak extends to the high-energy side, both along the excitation and the emission frequency, resulting in a triangular-like shape. At longer values of T, signals at cross-peaks positions become clearly distinguishable from the main peak especially on the upper diagonal portion of the maps (positions 4 and 7 in Figure 1b). While the spectral features along the diagonal are due to signal components in which the molecule is excited and emits at the same frequency ($\omega_1 = \omega_2$), cross-peaks indicate that an initially created coherence with

frequency ω_1 is coupled by successive interactions with the laser or by intramolecular dynamics to a different coherence with frequency $\omega_2 \neq \omega_1$. The progression of the signal as a function of T gives further information on the coherences excited in the system.

For the design of the logic implementations discussed below, we studied the dependence of the signal intensity on T at the location of seven points marked in the map in Figure 1b. The points 1, 7, 8, and 9 correspond to the frequency coordinates matching the maxima of the main transition (535 THz) and the vibronic shoulder (568 THz) of the linear absorption spectrum. Points 2, 3, and 4 were chosen in order to investigate the dynamics of the signal corresponding to the positions of the cross-peaks arising at longer values of T, where the laser spectral bandwidth provides higher amplitudes of the 2D-PE signal. Figure 1c reports the dynamics of the signal as a function of the population time T at the coordinates of point 2. The extracted trace exhibits oscillations superimposed on the decay dynamics. For a single chromophore, the presence of oscillations in the signal during T corresponds to the evolution of a vibronic coherence. The FT of these oscillations reveals the presence of several beating components in the low-wave-number region (<500 cm^{-1}) (see Figure 1c), whose frequencies cannot be reliably resolved. In addition, a dominant component at 660 cm^{-1} is clearly identified. This frequency matches, within the experimental error, the energy difference between positions 1 and 4 and corresponds to a strong vibrational mode identified in the Raman spectrum (see SI section 3). By Fourier transforming the set of 2D spectra across the population time T, the distribution of the beating components as a function of the (ω_1, ω_2) frequencies can be obtained. Figure 1d shows the spectral distribution of the 660 cm^{-1} beating component; it involves mainly the signal at the cross-peaks coordinates 2 and 4, whose positions are consistent with an excited-state vibrational mode.[14] We thus interpret the dynamics at these coordinates as deriving from the evolution of the coherent superposition of the two transitions g $\rightarrow$ e$_0(\nu = 0)$ and g $\rightarrow$ e$_1(\nu = 1)$, oscillating at the frequency ($\omega_{e1g} - \omega_{e0g}$) (see the energy levels scheme in Figure 1 a). This level structure should lead to a diagonal peak at position 3 and a stronger cross-peak at position 2 in the 2D maps of Figure 1b.[15−18] Such signals are not clearly detected in the experimental maps, probably because of an absorption process to a higher excited state, which contributes with an opposite sign to the total signal in the same spectral region. Transitions to a higher electronic state are supported by the inspection of the real part of the signal, where a negative feature is clearly recognizable on the higher-energy side of the maps (see SI section 4.1). The position of this negative signal is in agreement with previously measured excited-state absorption (ESA) spectra of rhodamines.[5,6,19] On the basis of these results, we simulate the PE response of the TAMRA dye in terms of the dynamics of an electronic three-level system (g, e, f) including explicitly a vibrational mode ($\hbar\omega = 660$ cm^{-1}) of the excited state e (see the scheme in Figure 1a). Figure 1e shows that the main features exhibited by the experimental data can be recovered by computing the third-order polarization with a molecular Hamiltonian comprising three electronic states and including explicitly an excited state of a vibrational mode. The nature and the energy of the higher excited state (f) involved is not known, but the transition e $\rightarrow$ f is in the same spectral window of the transition g $\rightarrow$ e. The spacing $\Delta E(f - e_0(\nu = 0)) = \Delta E(e_0(\nu = 0) - g) + 760$ cm^{-1} recovers the main feature of the experimental spectra in the

simulated spectra (Figure 1e,f). The simulations of the 2D-PE spectra are performed with a nonperturbative approach[20,21] for solving the density matrix dynamics,[7,22] accounting for the effect of the limited laser bandwidth, (further details of the nonperturbative simulation are reported in section 5 of the SI). According to the four-level scheme shown in Figure 1a, the density matrix describing the system can be expressed as a linear combination of 16 observables, the projectors kj = |k⟩⟨j|, where the indices refer to the four states of the chromophore, Figure 1a, the ground, two singly excited, and one doubly excited, k,j = g,e_0,e_1,f. The diagonal elements, kk, are the populations, while the off-diagonal ones are the coherences. Each interaction with the laser connects an element of the density matrix to another. For example, the interaction with the first laser pulse ($-\mathbf{k}_1$) brings the system from the ground state (gg) to coherence states (ge_0 and ge_1). For the logic implementation discussed below, it is important to note that each such a change is bilinear. It is linear in the operator describing the state of the system, and it is linear in the laser field.

A graphical representation of the branching between the molecular states due to the interaction with the pulse sequence is shown in Figure 2a, while a more formal description is given
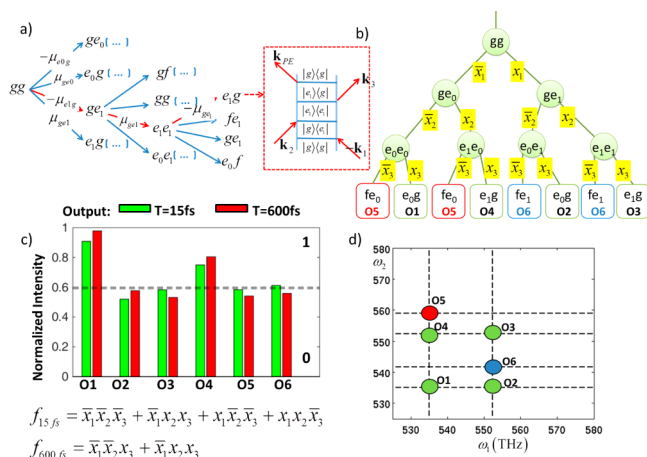

Figure 2. Parallel implementation of the decision trees of two three-variable Boolean functions on the 2D-PE molecular response. (a) Branching of the density matrix due to the interaction with the pulses. For the interaction sequence highlighted in red, the corresponding Feynman diagram is shown. (b) Logical decision tree representing the class of the three-variable Boolean function implemented in the system dynamics. The spectral positions of the output reading are indicated in the terminal nodes (leafs). (c) Outputs obtained from the experimental spectra of Figure 1, for two different population times, by reading the spectral intensities in the spectral region indicated in (d). The corresponding functions are written in terms of their min-term expansion.

in section 6 of the SI. A specific sequence of elements of the density matrix coupled with the time-ordered interactions with the laser pulses identifies a unique Liouville pathway. In terms of perturbation theory, such a sequence can be represented as a double-sided Feynman diagram, as illustrated in Figure 2a. In the SI, we report all 12 pathways contributing to the spectra of DNA_TAMRA. The spectral regions where ESA pathways contribute are identified by points 5 and 6 in the spectra of Figure 1b.

A binary decision tree defines a Boolean function by giving the outputs that correspond to all possible inputs. When

implemented in parallel, it gives all of the possible outputs simultaneously. The core idea for the parallel implementation of a molecular decision tree by the system dynamics is the branching between the states of the system due to their interaction with the pulses, as shown in Figure 2a.[10] Each time the pulse interacts with the molecule, another logic input of the function is resolved, which corresponds to a new subtree in the decision tree. The response of the system depends both on the value of the input and on its dynamical state when it interacts with the pulse. Therefore, the device operates as a finite state machine and not as a simple gate. This point is essential for the implementation of the decision tree.

Figure 2b shows the binary tree implemented on the third-order response function of TAMRA_DNA. The two values of a Boolean logic variable, say TRUE and FALSE, are physically encoded into the outcome of the laser-induced transition, namely, "does the laser excite a specific transition". Because we are considering here the response to a sequence of three laser pulses, the outcomes resulting from the action of the three laser pulses define the $8 = 2^3$ possible assignments of three logic variables, x_1, x_2, and x_3. A Liouville pathway corresponds to a specific assignment for x_1, x_2, and x_3 and contributes to a specific spectral region in the 2D maps where the value of the output is read. Therefore, a total of 8 Liouville pathways is necessary for the implementation of the decision tree of a three-variable Boolean function.

The first interaction assigns the value of the first logic proposition, x_1, to the vibrational mode being excited by the interaction with the first laser pulse. Two subtrees are generated depending on the value of x_1; for x_1 = true, the ge_1 coherence is created, while for not(x_1) = true, the system is described by ge_0 coherence. The second laser assigns the value of the second logic proposition x_2 as the vibrational mode being excited by the interaction with the second laser pulse. Depending on the value of x_2 and on the previous state of the system, the new state is either a population in a given vibrational state of the excited state (e_0e_0, e_1e_1) or a vibrational coherence (e_0e_1, e_1e_0). The third laser assigns the value of the proposition x_3 to the interaction with the laser stimulating the system to emit. The branches of the tree ending with x_3 = TRUE represent the four stimulated emission (SE) contributions, while the branches ending with x_3 = FALSE are the four ESA pathways. The set of ground-state bleaching (GSB) pathways bring a constant contribution to the measured spectra because the system is in the ground state during the population time T. Because they do not bring any dynamics in the spectrum, they are not included in the logic implementation.

The values of the outputs of the logic function are reported at the leaves (terminal nodes) of the logic tree shown in Figure 2b. Each leaf corresponds to the output of the function for the inputs that constitute the path from the root to the leaf. The values of the outputs are read at specific locations on the 2D map marked O1−O6 in Figure 2d. Because the detected signal is made up of all of the Liouville pathways, a single 2D map provides the evaluation of the logic function for all of the possible input strings in parallel. Each pathway contributes to one of the six spectral regions O1−O6, namely, O1(ω_{e0g},ω_{e0g}), position 1 in the spectrum of Figure 1b, O2(ω_{e1g},ω_{e0g}), position 2, O3(ω_{e1g},ω_{e1g}), position 3, O4(ω_{e1g},ω_{e0g}), position 4, O5(ω_{e0g},ω_{fe0}), positions 5, and O6(ω_{e1g},ω_{fe1}), position 6. The assignment of the relative intensities to Boolean values at these six positions is shown in Figure 2c. Because two Liouville pathways contribute to the positions O5 and O6, one can only

compute decision trees for a restricted class of the $2^{2^3} = 256$ Boolean functions of three variables, which are such that the Boolean outputs for the branches $\bar{x}_1, \bar{x}_2, \bar{x}_3$ and $\bar{x}_1, x_2, \bar{x}_3$ for O5 and $x_1, \bar{x}_2, \bar{x}_3$ and $x_1, x_2, \bar{x}_3$ for O6 are the same. By tuning the population time T, it is possible to design which of the $2^6 = 64$ logic functions is implemented. We show in Figure 2c the implementation of two such Boolean functions corresponding to $T = 15$ and 600 fs, for which the spectra are shown in Figure 1b. The experimental error in the reading of the relative intensities is estimated to be 1% from repeated measurements, allowing an accurate assignment of the truth value of the outputs.

The well-defined relative intensities that can be measured at different positions also allow for multivalued implementations. We report such a realization, using the fact that n-variable, m-output switching functions $(f_0, f_1, ..., f_{m-1})$ can be represented by a unique integer-valued function (Z) whose values at $x = (x_1, ..., x_n)$ are given by $f_z(x) = \sum_{i=0}^{m-1} f_i(x_1, ..., x_n) 2^i$.[23] The representation of m-output Boolean functions at the integer level is of interest because it is more compact. For example, to represent a two-output Boolean function, one needs to read one four-valued output only. As an example, we will consider the half addition of two binary digits, x_1 and x_2. This operation, whose truth table is shown in Figure 3a, delivers two outputs;
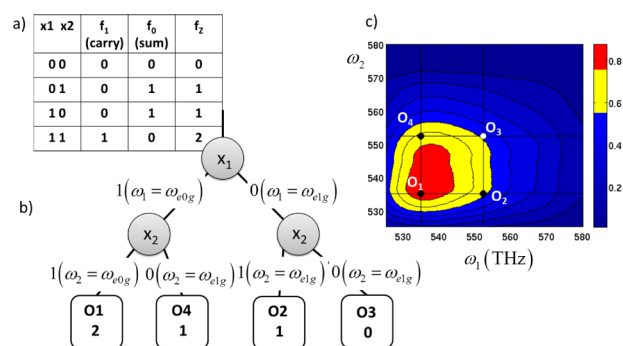

Figure 3. Example of implementation of a multivalued logic. (a) Truth table of the two-inputs/two-outputs addition function and integer representation of the output $f_Z = f_1(x_1, x_2)2^1 + f_0(x_1, x_2)2^0$. (b) The corresponding multiterminal logic tree, with the terminal nodes (leafs) showing the spectral position for reading the arithmetic output. (c) Experimental 2D-PE spectra for $T = 435$ fs; the color-code shows the three-valued reading of the output.

the output function f_0 is the sum modulo of two of the two input variables, while the output function f_1 is the carry to be transmitted for the addition of the next digit. By using the integer representation, $f_Z = f_1(x_1, x_2)2^1 + f_0(x_1, x_2)2^0$, the two-output function can be expressed as a function taking values on the finite set $Z = (0, 1, 2)$. Therefore, the reading of the intensities has to be mapped into three values. The binary logic tree for the addition of two Boolean variables x_1 and x_2 in the integer representation is shown in Figure 3b. It is a multiterminal decision tree that admits integer values in the terminal nodes. We implement the addition tree in the 2D-PE spectrum by lumping the Liouville pathways characterized by the same frequency during the coherence time τ, defining the variable x_1, and during the detection time, t, which defines the variable x_2. In the case of two variables, only four positions on the map are needed to read the outputs. Therefore, the outputs are read in the diagonal and cross-peak positions O1, O2, O3, and O4 of Figure 2d.

We show in Figure 3c that the half adder function is implemented accurately by the dynamics at a population time $T = 435$ fs. The main diagonal peak in the 2D map, at position O1, corresponds to the output for $(x_1, x_2) = (1,1)$ and to the highest arithmetic value 2 of f_Z; the two cross-peaks (in positions O4 and O2 corresponding to inputs $(1,0)$ and $(0,1)$, respectively) and output $f_Z = 1$ and the high-frequency diagonal peak (O3) correspond to inputs $(0,0)$ and $f_Z = 0$. The map of all possible outputs of the addition of two Boolean variables has therefore been obtained in parallel using an integer representation and a multivalued output.

In summary, we demonstrate the implementation of parallel and multivalued logic operations in the experimentally probed 2D-PE of a rhodamine dye mounted on a DNA double helix. Parallel processing is enabled by the dynamics resulting from the coherent excitation of multiple vibronic transitions between the energy levels of the chromophore upon interactions with the femtosecond laser pulses. The ability to read multiple outputs in parallel in the 2D-PE spectra allows for the simultaneous evaluation of all of the outputs of a logic function of three variables in a single experiment. The number of variables of the logic function is determined by the number of pulses in the setup. Each triplet of inputs corresponds to a dynamic Liouville pathway of the density matrix of the system. The computation of the 256 Boolean of three variables would therefore require one to resolve eight positions. With the present setup, a maximum of 64 functions could in principle be computed by tuning the values of the population time T at which the outputs are measured, provided that the vibronic dynamics can be resolved to provide the required outputs. We demonstrate here the implementation of two such functions. By a multiple-valued reading of the spectral intensities, we show that it is possible to go beyond a binary representation and implement directly parallel arithmetic logic. The characterization of vibronic dynamics allowed to physical implementation of these complex parallel logic operations on a single dye. More complex dynamics, including an intramolecular cascade between two chromophores mounted in the same DNA scaffold and reconfigurable devices obtained by inducing isomerization of the optically active units through chemical stimuli (e.g., pH change), will allow one to realize more complex parallel logic operations.

■ ASSOCIATED CONTENT

Ⓢ Supporting Information

Experimental setup, linear characterization, Raman spectrum, simulation methodology, and supplementary figures, including structures of species used, frequency-resolved optical gating map time intervals and excitation schemes in 2D photon echo spectroscopy, absorption and fluorescence emission spectra, resonance Raman spectra, experimental rephasing 2D maps, and Feynman diagrams. This material is available free of charge via the Internet at http://pubs.acs.org.

■ AUTHOR INFORMATION

Corresponding Author

*E-mail: FRemacle@ulg.ac.be or rafi@fh.huji.ac.il.

Notes

The authors declare no competing financial interest.

◾ REFERENCES

(1) Kompa, K. L.; Levine, R. D. A Molecular Logic Gate. *Proc. Natl. Acad. Sci. U.S.A.* **2001**, *98*, 410–414.

(2) Raymo, F. M.; Giordani, S. All-Optical Processing with Molecular Switches. *Proc. Natl. Acad. Sci. U.S.A.* **2002**, *99*, 4941–4944.

(3) Shi, W.; Fu, Y.; Li, Z.; Wei, M. Multiple and Configurable Optical Logic Systems Based on Layered Double Hydroxides and Chromophore Assemblies. *Chem. Commun.* **2015**, 711–713.

(4) Fassioli, F.; Oblinsky, D. G.; Scholes, G. D. Designs for Molecular Circuits That Use Electronic Coherence. *Faraday Discuss.* **2013**, *163*, 341–351.

(5) Remacle, F.; Speiser, S.; Levine, R. D. Intermolecular and Intramolecular Logic Gates. *J. Phys. Chem. A* **2001**, *105*, 5589–5591.

(6) Kuznetz, O.; Salman, H.; Eichen, Y.; Remacle, F.; Levine, R. D.; Speiser, S. All Optical Full Adder Based on Intramolecular Electronic Energy Transfer in the Rhodamine–Azulene Bichromophoric System. *J. Phys. Chem. C* **2008**, *112*, 15880–15885.

(7) Remacle, F.; Weinkauf, R.; Levine, R. D. Molecule-Based Photonically Switched Half and Full Adder. *J. Phys. Chem. A* **2005**, *110*, 177–184.

(8) Margulies, D.; Felder, C. E.; Melman, G.; Shanzer, A. A Molecular Keypad Lock: A Photochemical Device Capable of Authorizing Password Entries. *J. Am. Chem. Soc.* **2006**, *129*, 347–354.

(9) Chen, K.; Schmittel, M. A Triple-Channel Lab-on-a-Molecule for Triple-Anion Quantification Using an Iridium(III)–Imidazolium Conjugate. *Chem. Commun.* **2014**, *50*, 5756–5759.

(10) Fresch, B.; Hiluf, D.; Collini, E.; Levine, R. D.; Remacle, F. Molecular Decision Trees Realized by Ultrafast Electronic Spectroscopy. *Proc. Natl. Acad. Sci. U.S.A.* **2013**, *110*, 17183–17188.

(11) Scholes, G. Light-Powered Molecular Logic Goes Nonlinear. *Proc. Natl. Acad. Sci. U.S.A.* **2013**, *110*, 17167–17168.

(12) Alhassid, Y.; Levine, R. Connection between the Maximal Entropy and the Scattering Theoretic Analyses of Collision Processes. *Phys. Rev. A* **1978**, *18*, 89–116.

(13) Pan, K.; Boulais, E.; Yang, L.; Bathe, M. Structure-Based Model for Light-Harvesting Properties of Nucleic Acid Nanostructures. *Nucleic Acids Res.* **2013**, 1–12.

(14) Turner, D. B.; Dinshaw, R.; Lee, K.-K.; Belsley, M. S.; Wilk, K. E.; Curmi, P. M. G.; Scholes, G. D. Quantitative Investigations of Quantum Coherence for a Light-Harvesting Protein at Conditions Simulating Photosynthesis. *Phys. Chem. Chem. Phys.* **2012**, *14*, 4857–4874.

(15) Egorova, D. Detection of Electronic and Vibrational Coherences in Molecular Systems by 2D Electronic Photon Echo Spectroscopy. *Chem. Phys.* **2008**, *347*, 166–176.

(16) Mančal, T.; Nemeth, A.; Milota, F.; Lukeš, V.; Kauffmann, H. F.; Sperling, J. Vibrational Wave Packet Induced Oscillations in Two-Dimensional Electronic Spectra. II. Theory. *J. Chem. Phys.* **2010**, *132*, 184515.

(17) Butkus, V.; Valkunas, L.; Abramavicius, D. Molecular Vibrations-Induced Quantum Beats in Two-Dimensional Electronic Spectroscopy. *J. Chem. Phys.* **2012**, *137*, 044513.

(18) Christensson, N.; Milota, F.; Hauer, J.; Sperling, J.; Bixner, O.; Nemeth, A.; Kauffmann, H. F. High Frequency Vibrational Modulations in Two-Dimensional Electronic Spectra and Their Resemblance to Electronic Coherence Signatures. *J. Phys. Chem. B* **2011**, *115*, 5383–5391.

(19) Speiser, S. Photophysics and Mechanisms of Intramolecular Electronic Energy Transfer in Bichromophoric Molecular Systems: Solution and Supersonic Jet Studies. *Chem. Rev.* **1996**, *96*, 1953–1976.

(20) Kato, T.; Tanimura, Y. Multi-Dimensional Vibrational Spectroscopy Measured from Different Phase-Matching Conditions. *Chem. Phys. Lett.* **2001**, *341*, 329–337.

(21) Seidner, L.; Stock, G.; Domcke, W. Nonperturbative Approach to Femtosecond Spectroscopy: General Theory and Application to Multidimensional Nonadiabatic Photoisomerization Processes. *J. Chem. Phys.* **1995**, *103*, 3998–4011.

(22) Mukamel, S. *Principles of Nonlinear Optics and Spectroscopy*; Oxford University Press: New York, 1999.

(23) Mano, M. M.; Kime, C. R. *Logic and Computer Design Fundamentals*; Prentice Hall: Upper Saddle River, NJ, 2000.